NASA Technical Memorandum 104547

Mechanical Properties of a Porous Mullite Material

Michael J. Viens

September 1991

NASA Technical Memorandum 104547

Mechanical Properties of a Porous Mullite Material

Michael J. Viens
Goddard Space Flight Center
Greenbelt, Maryland

NASA
National Aeronautics and
Space Administration

Goddard Space Flight Center
Greenbelt, MD

1991

TABLE OF CONTENTS

Mechanical Properties of a Porous Mullite Material

ABSTRACT

Modulus of rupture specimens were used to determine crack growth parameters of a porous mullite material. Strength testing was performed in ambient and moist environments. The power law crack growth rate parameters "n" and "ln B" in 50% relative humidity were foumd to be 173.6 and 0.93, respectively. The power law crack growth rate parameters "n" and "ln B" in a moist environment were foumd to be 44.98 and 0.94, respectively The inert strength, fracture toughness and elastic modulus were also determined and found to be 19 MPa, 0.55 MPa(m)$^{1/2}$, and 11.6 GPa, respectively. These values are lower than those predicted by theory based on the properties of dense mullite. Radiographic inspection of the MOR specimens revealed spherical and lamination voids, these types of voids are commonly found when the closed mold slip casting process is used. A design diagram providing the required proof test levels as a function of desired lifetime and applied stress for the porous mullite is also presented.

INTRODUCTION

Porous mullite material has been traditionally used as a filter in applications where its structural integrity was unimportant. This material is to be used in the Super Helium On Orbit Transfer (SHOOT) Experiment which is scheduled to be flown on the STS in January of 1993. The use of this material in flight requires that its load carrying capability be fully characterized and that the component reliability during lift off and service be insured via design safety margins and component screening techniques such as proof testing and non destructive inspections.

The SHOOT experiment will demonstrate a new technology intended to increase the lifetimes of cryogenically cooled spacecraft experiments. The experiment lifetimes will be prolonged by the resupply of liquid helium coolant to the experiment dewars from onboard tanks. At present, experiment lifetimes are limited by the rate at which the helium stored in the dewars escapes into space.

The on orbit pumping of liquid helium is made difficult by its small molecular size, the liquid helium molecules slip past any type of mechanical seal. The absence of gravity on orbit prevents using the gravity feed pumping which is used on earth. The technology being developed by the SHOOT program is a thermally activated transfer of liquid helium through a porous medium. A porous mullite (Coors Ceramic Co., Golden CO) material acts as the pumping medium (Figure 1).

The primary purpose of the testing performed was to determine the strength distribution of the porous mullite and to determine the crack growth rate parameters of the porous mullite material in a moist environment. The strength distribution documented here represents that of the SHOOT experiment flight component.

THEORETICAL BACKGROUND

Rupture Strength

The modulus of rupture (MOR) specimens used in this study were tested in four point loading. The support span of 5.08 cm, a loading span of 1.693 cm, and the rectangular cross section of the MOR bars yield an applied surface stress (σ) given as [1]:

$$\sigma=2P/bt^2 \quad (1)$$

where P is the total applied load, b is the specimen width and t is the specimen thickness.

Due to the large variability of failure strengths typically observed in glass and ceramic materials the strength data must be viewed in terms of failure probability. The strength data for each test condition are fitted to a two parameter Weibull distribution [2]:

$$\ln\ln[1/(1-F)]=m\ln[\sigma_f/\sigma_o] \quad (2)$$

where σ_f is the applied stress at failure, and m and σ_o are the Weibull modulus and Weibull scale parameter, respectively. The Weibull parameters are determined by a least squares linear regression of Eq. (2), where F is the cumulative failure probability defined as, F=(i-0.5)/J (i is the specimen rank and J is the total number of specimens tested). The Weibull median strength is the failure strength corresponding to a failure probability of 0.5. The Weibull modulus represents the scatter in specimen strength where a low value indicates a greater variation in failure strengths.

The Weibull constants can be used to predict the failure probability of large components based on the strength distribution of the test specimens [3]. The predicted strength of a large component is obtained by scaling the small test specimen strength at an acceptable level of failure probability. The location of the strength controlling flaws (i.e. volume or surface) and the stress distribution must be taken into account when determining component failure probability.

Fracture Toughness

The specimen strength can be related to the inherent flaw size using the general stress intensity (K_I) relationship [4]:

$$K_I = Y\sigma\sqrt{a} \quad (3)$$

Where Y is a crack geometry term taken to be 1.12 for half penny shape surface flaws and *a* is the crack radius. When σ is the failure stress σ_f, K_I becomes the critical stress intensity K_{IC}.

The fracture toughness was determined according to ASTM E399 using notched bend specimens. The critical stress intensity or fracture toughness (K_{IC}) is given as :

$$K_{IC}=(PS/BW^{3/2})\, f(a/W) \quad (4)$$

where P is the applied load, S is the support span, B is the specimen width, W is the specimen thickness and f(a/W) is a geometric parameter whose values are given in ASTM E399.

Crack Growth

Environmentally assisted crack growth in glass and ceramic materials, also referred to as static fatigue, occurs when the material is stressed in moist environments. The rate of crack growth can be expressed as a power law relationship between applied stress (σ_a) and time to failure (t_f), given as [5]:

$$t_f = B\sigma_i^{n-2}\sigma_a^{-n} \tag{5}$$

where σ_i is the inert strength, σ_a is the applied stress, and n and B are material and environmental crack growth constants. Inert strength is the strength in the absence of subcritical crack growth. The crack growth parameters n and B are determined by fatigue testing. Static fatigue testing determines the median time to failure as a function of the applied stress. The use of the median values is convenient as they represent the time to failure at a 50% failure probability. A least squares linear regression is performed on the natural logs of the Weibull median times to failure and the corresponding applied stresses. The slope is the n parameter and the intercept is $\ln(B\sigma_i^{n-2})$.

The loading described in Equation (5) is static loading at a constant applied stress. While this type of loading does often correctly simulate the type of loading experienced in service, the determination of crack growth constants with this technique is time consuming. An alternate method to determine crack growth constants which requires less time is that of dynamic loading. The relationship between applied stress at failure (σ_f) and stressing rate ($\dot{\sigma}$) is given as [5]:

$$\sigma_f^{(n+1)} = B(n+1)\,\sigma_i^{n-2}\dot{\sigma} \tag{6}$$

The crack growth constants are determined as described for static fatigue using the median failure stresses and the associated stressing rates.

The time to failure of a component can be calculated with equation (5) using the inert strength at an acceptable level of failure probability. This inert strength must be scaled to reflect the component size and stress distribution. An alternate approach to insuring the survival of the component is to proof test components prior to service. The proof test will require loading the service component to some load greater than the service load. The probability of surviving the proof stress (σ_p) is calculated by Eq. (5) replacing the inert strength with the proof stress. The minimum time to failure is then calculated as [6]:

$$t_{min} = B\sigma_p^{n-2}\sigma_a^{-n} \tag{7}$$

This design approach eliminates the need to determine the acceptable in service failure probability and the decision is shifted to determining an acceptable proof test failure probability. The latter approach is preferred as a failure during launch would compromise the mission.

EXPERIMENTAL PROCEDURE

Material

The material used to manufacture the thermomechanical pumps is a porous mullite material. Mullite is nominally 60% Al_2O_3 and 40% SiO_2. The specimens were made from a mullite slurry and slip cast in a closed mold which was then fired at 1000°C. This temperature is lower than that typically used to sinter mullite and was used to maintain the porosity in the mullite by minimizing liquid flow. The manufacturer's[1] data for this material, designated as P-1/2B-C, is listed in Table 1.

The apparent density was measured on several specimens and found to be 1.726 g/cc with a standard deviation of 0.0245 g/cc. The material volume fraction pores was calculated as one minus the ratio of apparent density to the density of mullite and was found to be 38%. This value agrees with the manufacturers value for apparent porosity.

Table 1.Physical Properties of Porous Mullite (P-1/2B-C)

MOR Strength(ksi)	3.0
Pore Diameter(um)	<0.5
Bubble Pressure (psi)	>80
Apparent Porosity	34.3%
Absorption	19.3%
Maximum Working Temperature (F)	1700
Specific Gravity	1.8

Manufacturer's data

Test Specimens

The test specimens were rectangular modulus of rupture (MOR) bars, nominally 63.5 mm (2.5") long, 12.7 mm (0.5") wide and 6.35 mm (0.25") thick. The specimens were randomized upon receipt to eliminate systematic errors due to manufacturing variables.

All specimens were x-ray radiographed upon receipt. The specimens were radiographed in a flatwise orientation at 80 cm source to film distance with 35 KV, 2.5 milliamps for 4 minutes on Kodak type M2 film. Specimens radiographed from the side used 45 KV, 4 milliamps for 2.5 minutes at a 80 cm source to film distance.

The presence of voids was determined by optical examination of the x-ray film, without magnification. An image of the area containing the detected void was captured at 50 times magnification and the area of each void was measured individually using an image analysis program[2]. The periphery of each void was marked by the operator and the inscribed area measured. Void diameter was calculated assuming the voids to be spherical.

[1]Coors Ceramic Co., Golden CO

[2]NIH Image

Tests

Strength testing was performed on a servo hydraulic test machine[3]. The inert and crack growth specimens were loaded in four point bending with a 50.8 mm (2") support span and a 16.9 mm (2/3") loading span. The bend fixture was mounted on the hydraulic ram and each specimen was put into contact with the loading span prior to ram engagement to avoid impact type loading. A piezoelectric load cell[4] was used to monitor loads at ram rates greater than 0.2 mm/sec. A standard strain gauged load cell[5] was used at rates less than 0.2 mm/sec. Load traces were recorded on a digitizing pen plotter[6].

Inert test strength specimens were dried in a vacuum at 50°C for 24 hours prior to testing. The measured weight loss due to moisture loss was found to be 0.217% +/- 0.040% by weight. The inert specimens were tested at a ram speed of 1.3 mm/sec.

Crack growth testing was performed on specimens soaked in distilled water and specimens stored under ambient conditions. The specimens were loaded at ram speeds between 0.13 mm/sec and 0.038 mm/hr.

The precracks in the fracture toughness specimens were prepared by first machining a 0.635 cm deep groove with a 0.191 cm wide diamond wafering tool. The sharp crack was created with 76 μm wire. The wire tended to create a slightly rounded crack front. The fracture toughness specimens were dried as described above and loaded in three point loading with a two inch support span at a ram speed of 0.8 mm/sec.

RESULTS

Radiographic Inspection

Radiographic inspection revealed a significant number of large voids in the test bars. There were two types of voids present; spherical voids and flat voids with tapering widths. The spherical voids are created by air trapped in the slurry when the mold is closed. The flat voids are called lamination voids and occur at the center of the cross section when the moisture in the slip is drawn out in opposite directions during casting. The density is generally slightly lower in the center of components manufactured using closed mold slip casting. Examples of these voids are shown in Figures 2 and 3.

Of the 500 specimens received 6.6% (33 specimens) had large lamination voids. These specimens were removed from the test lot. Of the 467 remaining specimens, 113 specimens had a total of 154 voids ranging in diameter from 0.36 mm to 4.6 mm. The size distribution of the spherical voids detected is shown in Figure 4. The majority of the spherical voids were located outside the loading span. Six specimens were noted to have voids within the loading span and near the surface. These specimens were tested under inert conditions to determine if failure would occur at the voids. Any specimens that failed from voids noted in radiographs were not used for the calculation of statistical parameters.

---

[3]Instron 1350, Instron Corp., Canton, MA
[4]Kistler Instrument Corp., Amherst, NY
[5]Eaton Corp., Troy, MI
[6]HP7090A, Hewlett Packard, San Diego, CA

Figure 4 indicates that the most common void size lies between 0.5 and 0.75 mm. It is felt that the number of voids less than 0.5 mm diameter is greater than those between 0.5 and 0.75 mm diameter but are too small for the radiograph and/or the inspector to consistently discern. While voids smaller than 0.5 mm diameter can be detected, the threshold for detecting the spherical voids is assumed to be 0.5 mm. This void size is three orders of magnitude greater than the pore size.

Elastic Modulus

The properties determined from this study are listed with those of dense mullite in Table 2. The elastic modulus was determined by monitoring a strain gauge on the compressive face of 10 MOR specimens. These specimens were taken to failure but were not included in inert or fatigue strength data. The stress versus strain relationship is linear up to failure as shown in Figure 5. The modulus was found vary from 8.9 GPa to 16.7 GPa with a mean and standard deviation of 11.6 and 2.5 GPa, respectively.

Several models exist to predict the mechanical properties of porous materials based on dense material properties [7]. The relationship is generally expressed in terms of fractional properties. The fractional modulus is the ratio of the porous modulus to the modulus of the dense material. A literature survey of porous materials found fire clay to have the lowest fractional modulus as a function of volume fraction pores. At 38% volume fraction pores the fire clay has a fractional modulus of 0.16. The fractional modulus of the porous mullite tested in this study varied from 0.059 to 0.111. The failure of the model to correctly predict the properties of the porous mullite is due to a lack of information on the properties of dense mullite sintered at 1000°C. As stated previously dense mullite is typically sintered at higher temperatures (1700°C) which increases the material stiffness and strength.

Inert Strength

The inert strength results are listed in Table 3 and the Weibull parameters are listed in Table 4. A Weibull plot for the inert strength is shown in Figure 6. The wide range of strengths observed and the low Weibull modulus indicate that there is a large variation in the size of the failure initiating flaws.

Fracture Toughness

The average fracture toughness was found to be 0.547 $MPa(m)^{1/2}$ with a standard deviation of 0.097 $MPa(m)^{1/2}$. The fracture toughness of the porous mullite is much lower than that of the dense mullite. This difference is again felt to be due to the low sintering temperature rather than the porosity itself.

The initiating flaw sizes were calculated for the extreme inert strengths using Equation 3. The flaw was assumed to be a half penny shape surface flaw and the fracture toughness was taken to be 0.547 $MPa(m)^{1/2}$. The flaw sizes were found to range from 0.11 mm to 0.57 mm with a median value of 0.21 mm. While the size of these flaws should make them easily detectable on the fracture surface, the texture of the fracture surface has made the direct measurement of the initiating flaw size difficult. A typical fracture surface is shown in Figure 7. It is not clear if the failures originate at the specimen surface or subsurface.

Table 2. Mechanical Properties of Dense and Porous Mullite

	MOR Strength Strength (MPa)	Elastic Modulus (GPa)	Fracture Toughness (MPa$\sqrt{m}$)	Density (g/cc)
Dense Mullite†	170	150	2.0	2.8
Porous Mullite (P-1/2B-C)	19.3 (3.88)	11.6 (2.5)	0.547 (0.097)	1.726 (0.025)

Numbers in parenthesis represent one standard deviation.
† Coors Ceramic Co. Golden CO

Table 3. Strength Test Results

Test Condition	Stressing Rate (MPa/sec)	Number of Specimens	Average Strength (MPa)	Median Strength (MPa)	Strength Range (MPa)
Inert	598	55	19.28(3.88)	19.33	11.53-26.10
50% RH	8.15	21	15.50(3.46)	15.53	10.93-21.64
50% RH	7.3E-2	21	14.54(2.92)	14.37	9.11-18.87
50% RH	7.60E-4	21	14.70(2.19)	15.07	9.12-18.03
H_2O	81.4	33	16.16(4.15)	15.81	9.34-23.56
H_2O	0.91	33	13.96(3.30)	14.05	8.28-19.13
H_2O	7.1E-3	31	13.11(2.71)	14.22	8.79-16.75

Table 4. Weibull Parameters

Test Condition	Stressing Rate (MPa/sec)	Intercept	Weibull Modulus	σo (MPa)	Median Strength (MPa)	Correlation R^2
Inert	598	-17.67	5.820	20.82	19.55	0.960
50% RH	8.15	-14.74	5.219	16.86	15.72	0.885
50% RH	7.3E-2	-15.99	5.808	15.69	14.73	0.973
50% RH	7.60E-4	-20.79	7.559	15.65	14.91	0.979
H_2O	81.4	-13.26	4.615	17.69	16.34	0.936
H_2O	0.91	-13.16	4.832	15.24	14.12	0.945
H_2O	7.1E-3	-14.00	5.265	14.28	13.32	0.863

Of the six specimens that had detectable voids within the loading span only one failed at the void. Figure 8 shows the fracture surface of this specimen. The maximum stress intensity at each void was calculated using the void depth and radius measured from a side view radiograph of the specimens. The stress intensity was calculated assuming the void to be a penny shaped crack subjected to pure bending. The stress intensity solution is reproduced in Figure 9. The results of this calculation are shown in Table 5. The calculated void stress intensity of the specimen that failed at the void (#369) is 0.57 MPa$\sqrt{m}$ which is approximately equal to the measured fracture toughness of 0.55 MPa$\sqrt{m}$. The stress intensity of the other voids is less than the fracture toughness so failure from these voids would not be expected.

Table 5. Stress Intensity at Voids within Loading Span

Specimen ID	Void Radius (mm)	Distance from Surface (mm)	Failure Load (N)	Stress Intensity (MPa$\sqrt{m}$)
302	0.293	0.80	250	0.415
303	0.288	0.65	257	0.443
326	0.729	2.21	291	0.435
369*	0.858	1.07	197	0.569
444	0.505	1.93	204	0.283
457	0.415	1.12	207	0.365

* Failed at void

Crack Growth Parameters

The specimen strengths and Weibull parameters measured at each test condition are listed in Tables 3 and 4. The median Weibull strengths are plotted versus the stressing rate in Figure 10. The crack growth parameters, n and B, determined from the Weibull median values are listed in Table 6. While a literature survey did not locate crack growth rates for mullite in a moist environment, the crack growth rates of alumina and silica are well documented. The crack growth rate of the porous mullite in a moist environment was found to be consistent with that of alumina and silica.

Table 6. Crack Growth Parameters

	Test Condition	n	lnB
Porous Mullite	50% RH	173.6	0.930
Porous Mullite	H_2O	44.98	0.940
Fused Silica [9]	H_2O	38.7	-.---
Alumina [10]	80% RH	37.53	3.440

DISCUSSION

Two design methodologies are commonly used to design ceramic components: statistical analysis and proof testing [6]. The statistical lifetime prediction assumes that the initial flaw size is unknown. This uncertainty requires that an acceptable level of failure probability be selected. The difficulty with this approach is that no guideline for acceptable failure probability has been

established. The proof test approach establishes a known maximum possible flaw size and forces failure of weak components to occur during the proof test.

A useful tool in designing with glass and ceramic materials is the design diagram. Design diagrams generated with data from this study for the porous mullite are presented in Figures 11 and 12. The steep curves, denoting failure probability, are generated for the MOR bars and do not reflect the pump stress distribution. The location of these curves for the pumps is dependent on the stress distribution and area stressed. The shallow curves reflect various levels of proof testing and are dependent on the ratio of proof stress to applied service stress. The proof stress curves in Figure 11 are generated using the moist environment crack growth parameters. The proof stress curves in Figure 12 are generated using the 50% RH crack growth parameters. These curves can be used to determine the required proof stress level as a function of required component lifetime and applied stress.

The post proof test lifetime is a minimum time to failure based on the knowledge that a flaw that would cause failure during proof testing does not exist in the component. This allows the uncertainty of failure during service to be eliminated but does require the risk of failure during proof testing. The probability of failure during proof testing is calculated with Eq. 2 using parameters that reflect the proof test environment (i.e. stressing rate and ambient moisture). It is important to note that the service environment of the pumps is inert and crack growth might only occur during integration and testing of the pumps.

As an example the required proof stress for a component which is to subjected to a 10 MPa stress for five years in a moist environment will be determined. The required proof stress to applied stress ratio is taken directly from the design diagram and found to be 1.7. That indicates a proof stress of 17 MPa is required. The probability of failure during the proof test is calculated from Eq. (2) Taking m = 5.82, σ_f = 17 MPa and σ_0 = 20.82. The proof test failure probability F is found to be 0.265 or 26.5%. While this is a high failure probability, survival of the proof test will insure that the component will survive for the required lifetime.

In addition to the test specimens seven of the SHOOT pumps were x-ray radiographed to determine the component quality. The results of the inspection are presented in Table 7. Radiographic inspection of pumps revealed the presence of voids in several pumps with void sizes ranging from 0.36 mm to 1.28 mm in diameter. The variation of void density indicates that the manufacturing process could easily go out of control. While no voids were observed in one pump (2-2), 12 voids ranging in size from 0.36 mm to 1.12 mm where observed in another pump (1-1). Figure 13 shows a number of the voids located in pump 1-1. The closed mold slip casting process is extremely operator dependent. This inherent process variability requires that all components be radiographed prior to use to insure component integrity.

Table 7 Voids Found in SHOOT Pumps

Pump ID	Number of Voids	Diameter Range (mm)
1-1	12	0.36 - 1.11
1-2	1	1.12
2-1	2	0.81 & 1.01
2-2	0	
2-3	5	0.37 - 1.19
2-4	2	2 @ 0.51
2-5	5	0.56 - 1.28

CONCLUSIONS

Radiographic inspection of all porous mullite components should be performed to establish the component quality.

While the average inert strength of the porous mullite MOR specimens (19.33 MPa) was found to agree with that quoted by the manufacturer (20.7 MPa), the design strength of this material should be quite a bit lower. At ambient 50% RH the strength of the MOR bars at a 0.10 failure probability is 11 MPa.

Component proof testing should be performed to eliminate the uncertainty associated with the wide range of strengths observed.

If proof testing is not performed, both the maximum applied stress and the stress distribution should be known so that the lifetime calculations can be performed for the area of maximum stress and at voids.

Fracture analysis performed treating the spherical voids as penny shape cracks appears to correctly predict applied stress intensity. While the presence of voids is not necessarily cause for immediate rejection, the strength of the component at the void and time to failure at the applied stress at the void should be determined.

The porous mullite material is sintered at a temperature well below that of fully dense mullite. Existing models cannot predicted the mechanical properties of the porous mullite using the properties of the dense mullite.

ACKNOWLEDGEMENTS

The author would like to thank the SHOOT project for their support in providing both test specimens and manpower to complete this study. The author would also like to thank Diane Kolos and Pat Friedberg for their diligent radiographic support.

REFERENCES

1. M.F. Spotts, Design of Machine Elements, 5th Edition, Prentiss-Hall, (1978)

2. W. Weibull, "A Statistical Distribution Function of Wide Applicability," Journal of Applied Mechanics, [18] 293-297 (1951)

3. J.E. Ritter, Jr., "Probabilistic Fracture Mechanics," Review of Progress in Quantitative Nondestructive Evaluation, Vol 1, Ed by D.O. Thompson and D.E. Chimenti, Plenum Publishing Corp. (1982).

4. R.W. Hertzberg, Deformation and Fracture Mechanics of Engineering Materials, 2nd Edition, John Wiley and Sons (1983).

5. T.M. Heslin, M.B. Magida and K.A. Forrest, "A Method for Developing Design Diagrams for Ceramic and Glass Materials using Fatigue Data," NASA RP 1174, September 1986.

6. S.M. Weiderhorn and J.E. Ritter, Jr., "Application of Fracture Mechanics Concepts to Structural Ceramics", Fracture Mechanics applied to Brittle Materials, ASTM STP 678, S.W. Frieman, Ed., American Society for Testing and Materials, 1979, pp 202-14.

7. R.L. Coble and W.D. Kingery, "Effect of Porosity on Physical Properties of Sintered Alumina," Journal of the American Ceramic Society, 39 [11] 377-385 (1955).

8. G.C. Sih, Handbook of Stress Intensity Factors, Lehigh University, Bethlehem, PA, 1973

9. S. Sakaguchi, et al, "Delayed Failure in Silica Glass," Journal of Materials Science, Vol 17, pp.2878-86,1982.

10. J.E. Ritter, Jr and J.N. Humenik, "Static and Dynamic Fatigue of Polycrystalline Alumina," Journal of Materials Science, Vol 14, pp. 626-32, 1979.

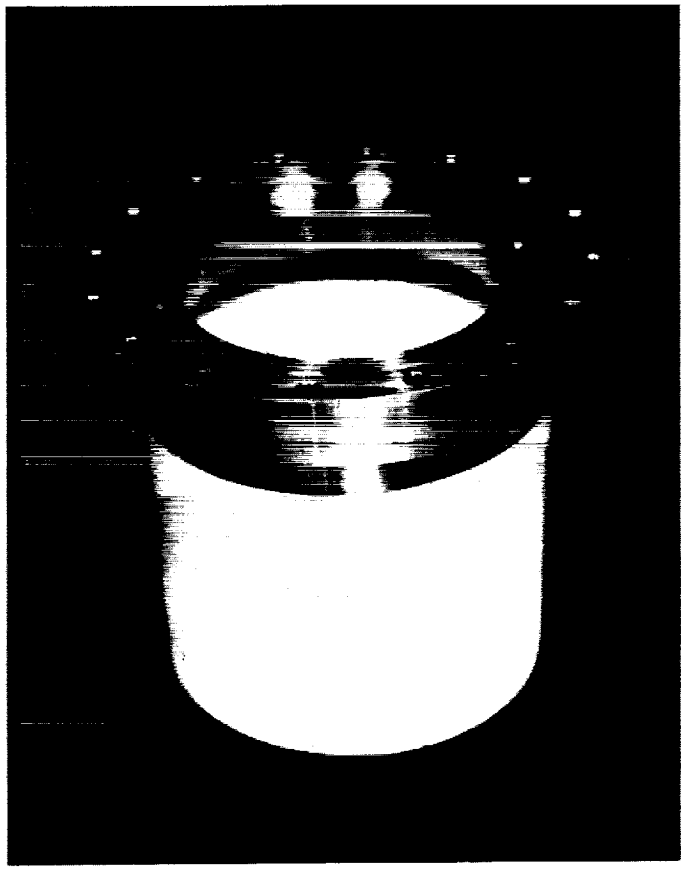

Figure 1. Porous mullite thermomechanical pump mounted in flange. Magnification 0.5 times.

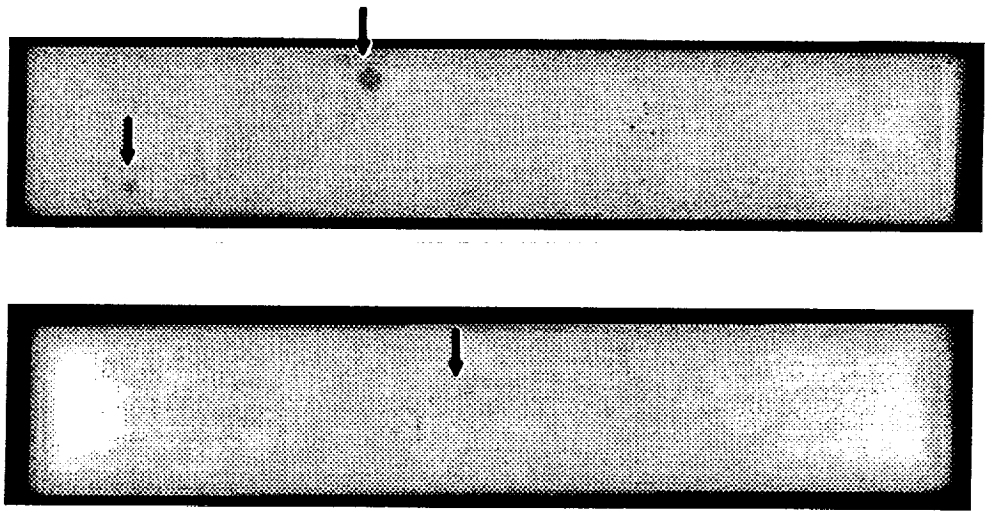

Figure 2 Spherical voids located in MOR bars. Top bar has large voids while lower bar has small void on the edge of the detection limit. Magnification 2 times.

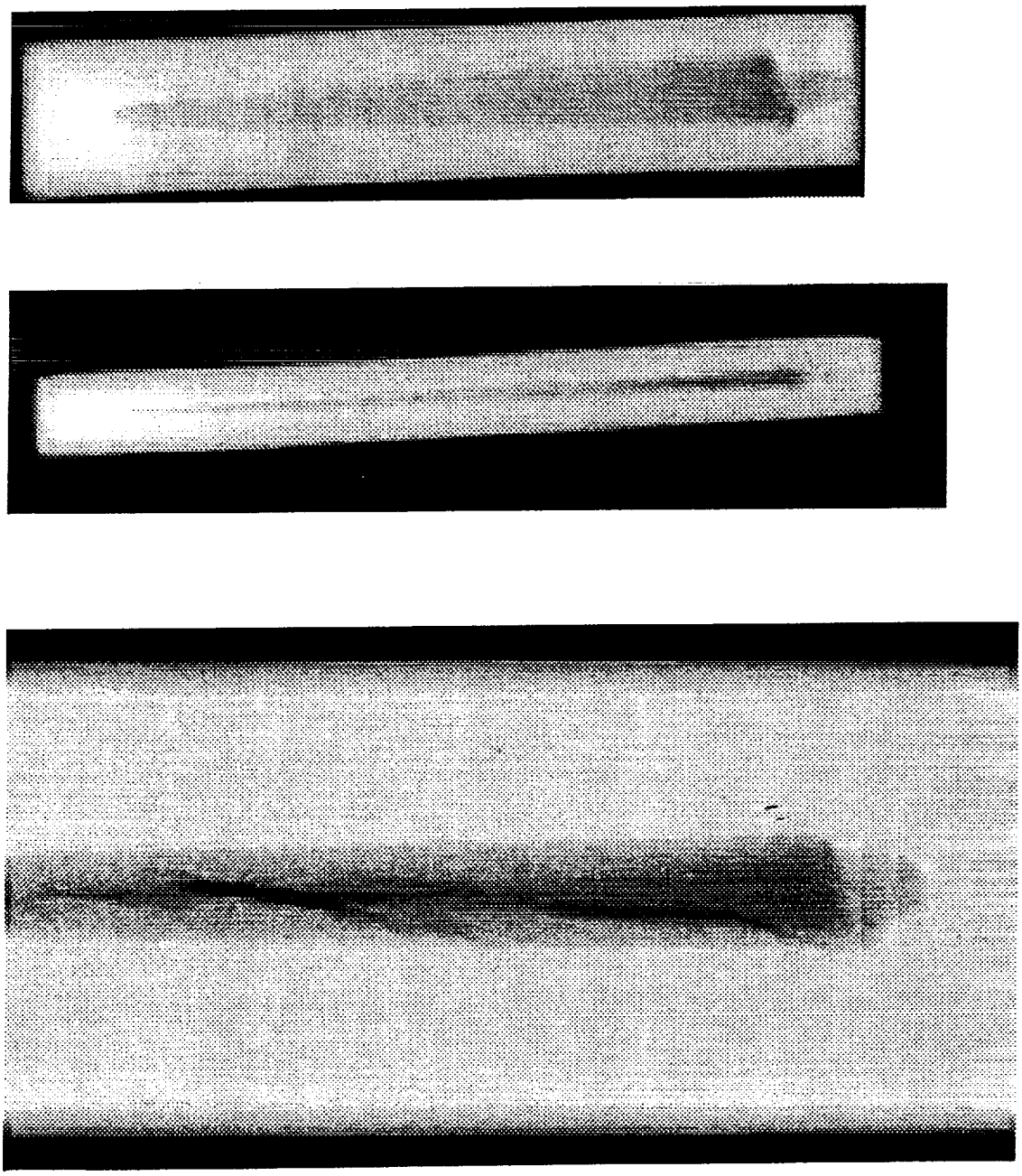

Figure 3 Lamination void. Top is a plan view and middle is a side view of the void at two times magnification . Bottom view is a close up of the side view at 12 times magnification.

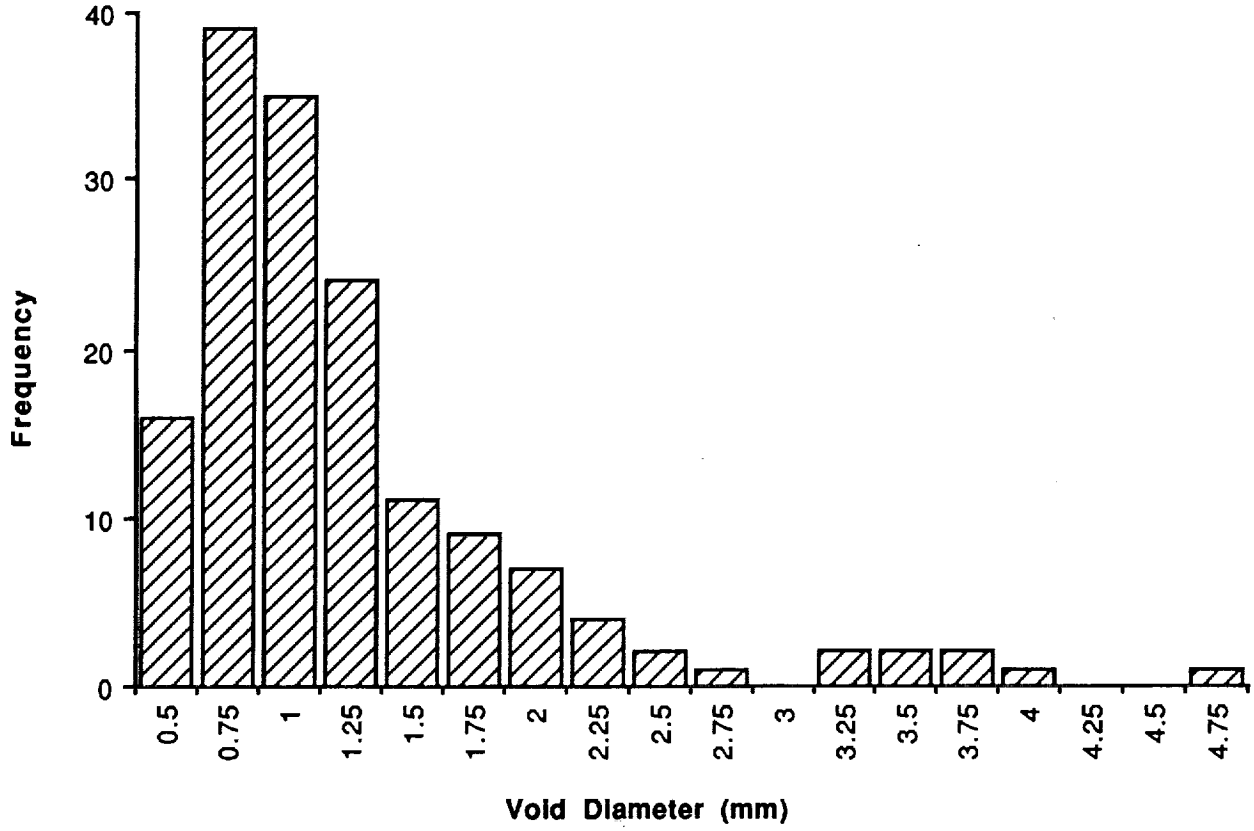

Figure 4 Histogram of the spherical voids located by radiography in the porous mullite MOR test specimens.

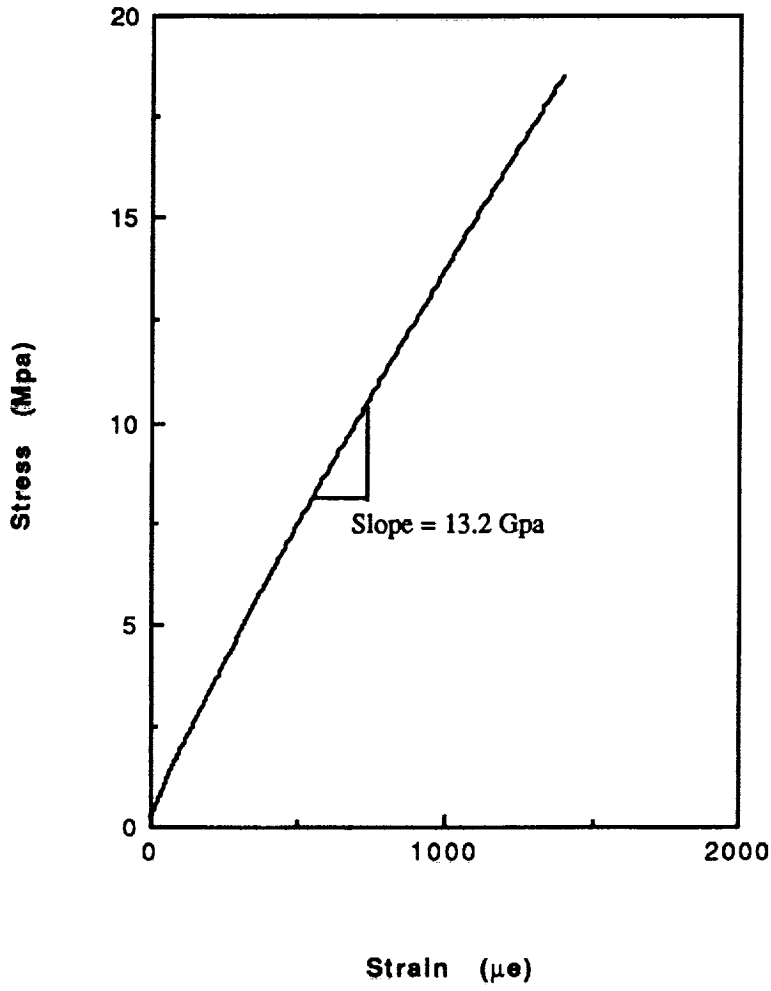

Figure 5. Typical stress versus strain curve for the MOR specimens.

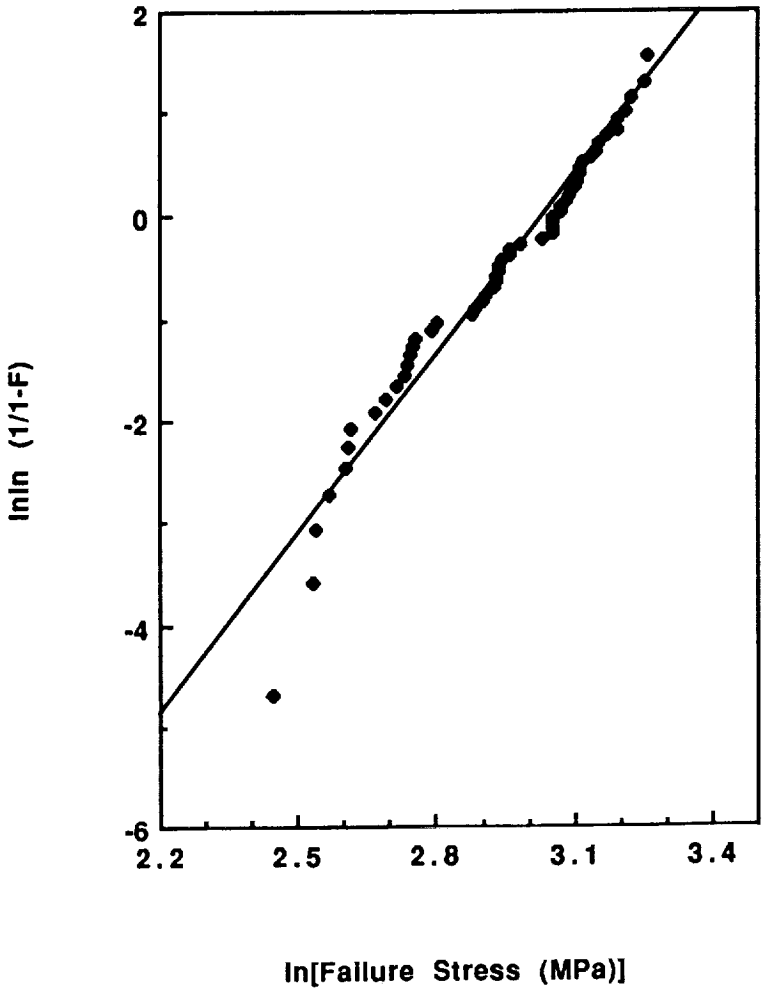

Figure 6. Weibull distribution for the inert strength specimens. The slope is the Weibull modulus (5.82).

ORIGINAL PAGE
BLACK AND WHITE PHOTOGRAPH

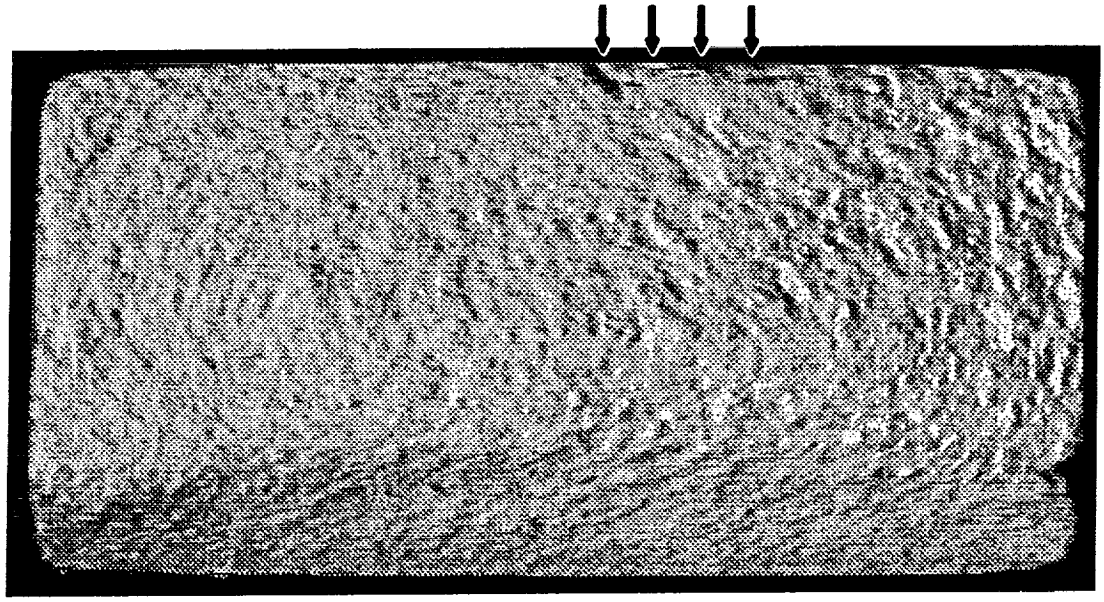

Figure 7. Typical fracture surface. Fracture origin appears to be in the center of the upper specimen face. Magnification 11 times.

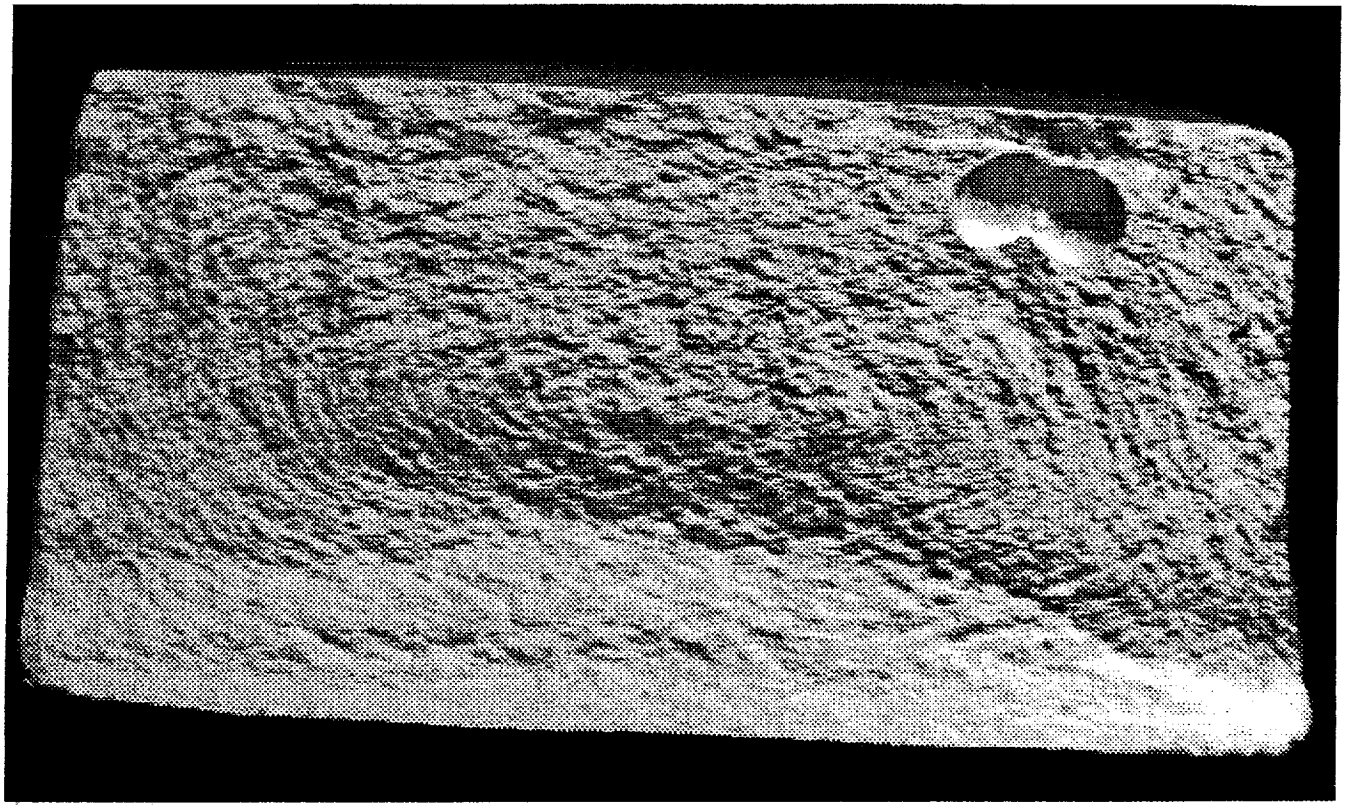

Figure 8 Fracture surface of specimen S/N 369. Magnification 13 times.

A Penny-Shaped Crack in a Beam Subjected to Pure Bending

(Smith, Kobayashi and Emery [1967])

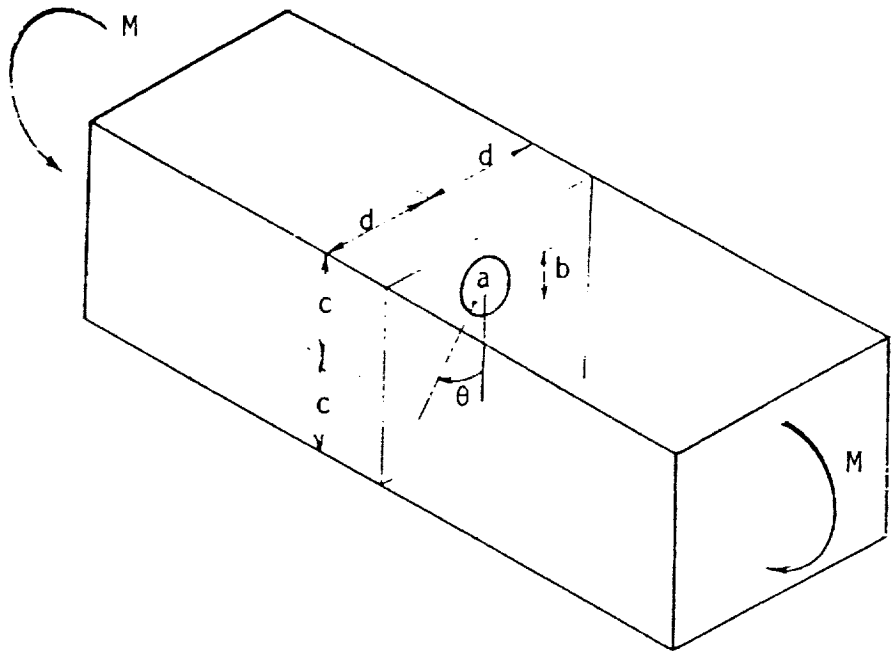

A prismatic beam of rectangular cross-section containing a small circular penny-shaped crack of radius a in a transverse section is subjected to pure bending as shown in the above figure. The interaction of the crack with the lateral surfaces of the beam can be neglected if d>3a and c-b>3a. The stress intensity factor can be written in the following form when $b > \frac{2}{3}a$:

$$k_1 = \frac{2}{\pi}\frac{a}{I}\left[\frac{b}{a} - \left(\frac{2}{3}\right)\cos\theta\right] M\sqrt{a}$$

where

$$I = \frac{2}{3} dc^3$$

Figure 9. Stress intensity solution used to analyze detected voids. Reproduced with permission from reference 8.

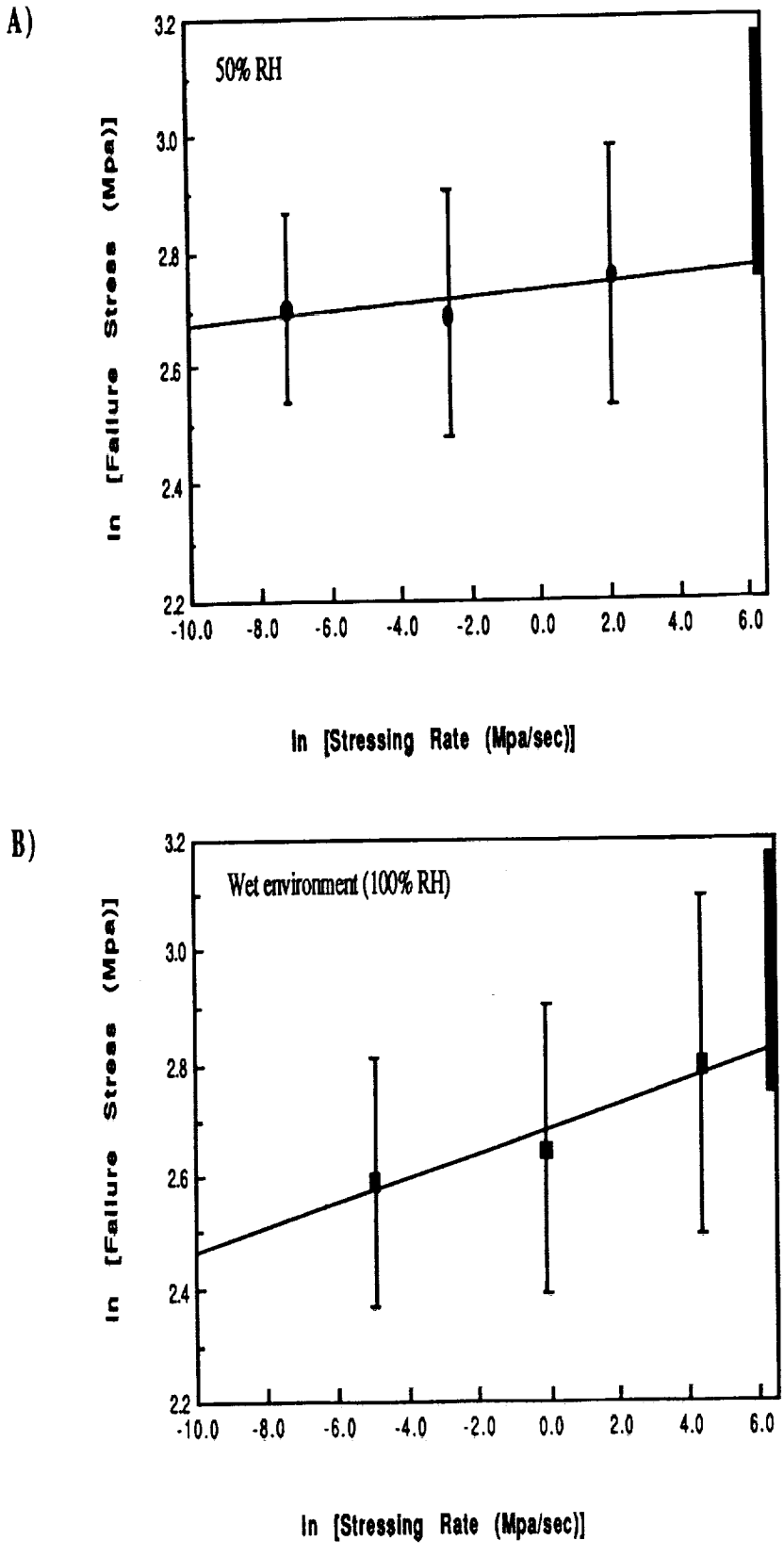

Figure 10. Dynamic fatigue data. A) 50% RH Weibull median strengths and B) wet (100% RH) environment data. The slope of the best fit straight line is the fatigue parameter n.

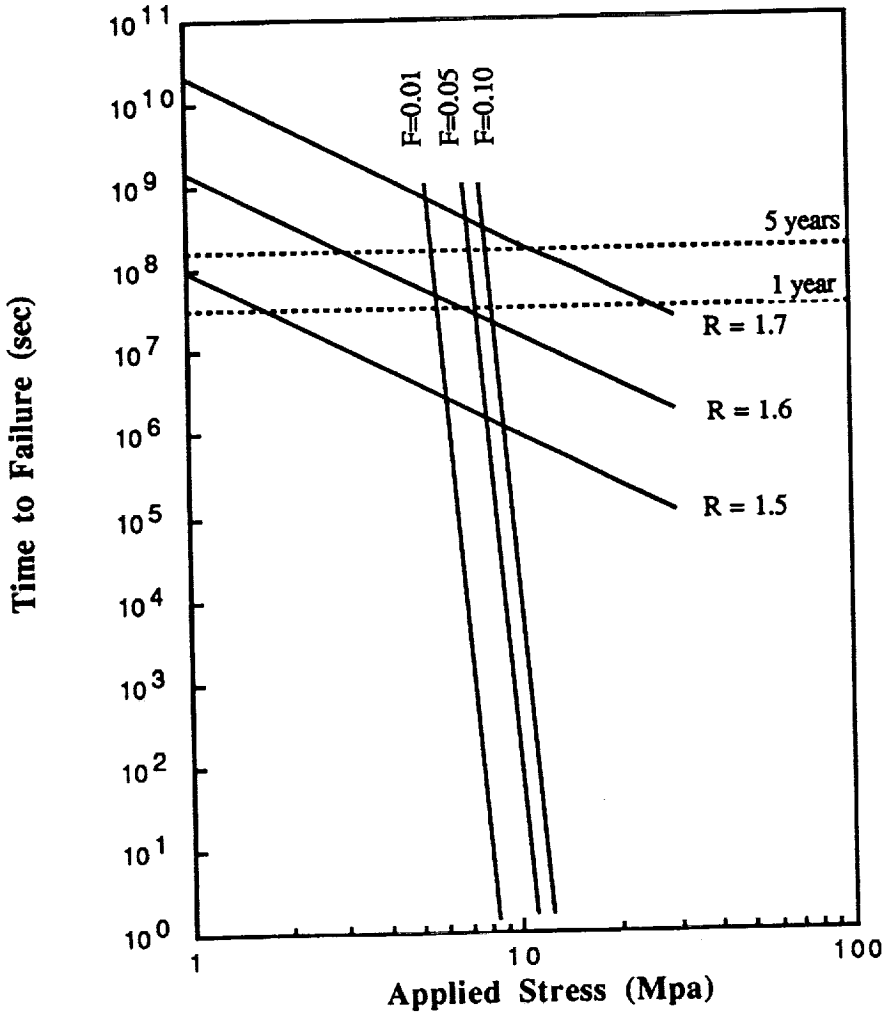

Figure 11. Design diagram for porous mullite in a wet environment. The shallow curves correlate minimum time to failure with applied service stress as a function of proof stress. R values represent the ratio of proof stress to applied service stress. The steep curves represent the time to failure as a function of applied stress for various levels of failure probability for MOR bars.

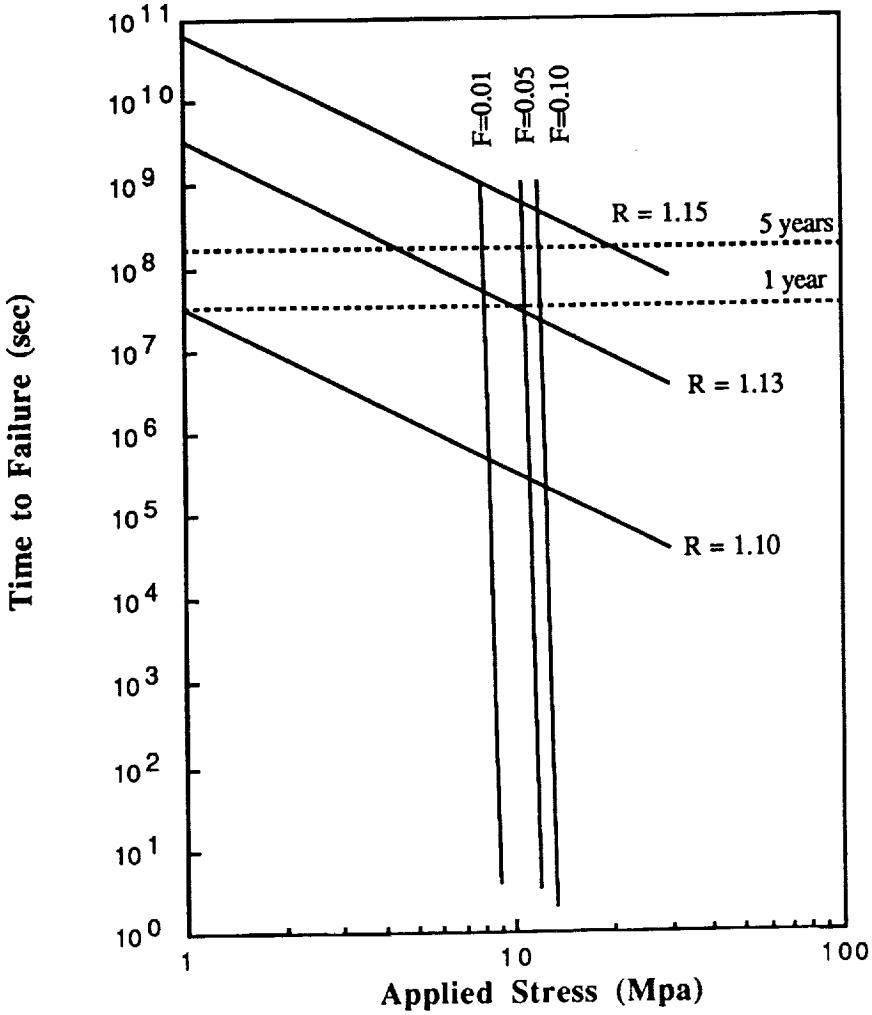

Figure 12. Design diagram for porous mullite in 50% relative humidity environment. Curves are as described in Figure 11.

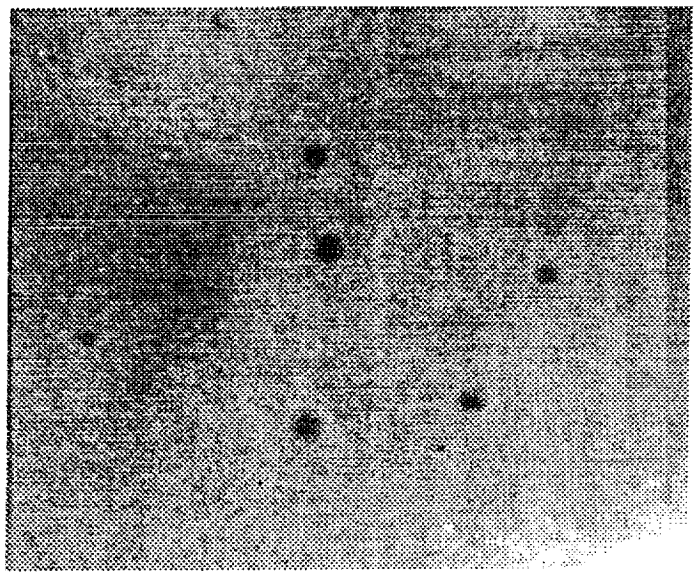

Figure 13 Several of the voids detected in S/N 1-1 pump. Magnification 10 times.

NASA
National Aeronautics and Space Administration

Report Documentation Page

1. Report No.	2. Government Accession No.	3. Recipient's Catalog No.
NASA TM 104547		

4. Title and Subtitle	5. Report Date
Mechanical Properties of a Porous Mullite Material	August 1991
	6. Performing Organization Code: 300

7. Author(s)	8. Performing Organization Report No.
Michael J. Viens	91B00143
	10. Work Unit No.

9. Performing Organization Name and Address	11. Contract or Grant No.
Goddard Space Flight Center Greenbelt, Maryland 20771	
	13. Type of Report and Period Covered: Technical Memorandum

12. Sponsoring Agency Name and Address	14. Sponsoring Agency Code
National Aeronautics and Space Administration Washington, D.C. 20546-0001	

15. Supplementary Notes

Michael J. Viens: NASA-GSFC, Greenbelt, Maryland, 20771.

16. Abstract

Modulus of rupture specimens were used to determine crack growth parameters of a porous mullite material. Strength testing was performed in ambient and moist environments. The power law crack growth rate parameters "n" and ln B" in 50% relative humidity were found to be 173.6 and 0.93, respectively. The power law crack growth rate parameters "n" and "ln B" in a moist environment were found to be 44.98 and 0.94, respectively. The inert strength, fracture toughness and elastic modulus were also determined and found to be 19 MPa, 0.55 MPa(m)$^{1/2}$, and 11.6 GPa, respectively. These values are lower than those predicted by theory based on the properties of dense mullite. Radiographic inspection of the MOR specimens revealed spherical and lamination voids, these types of voids are commonly found when the closed mold slip casting process is used. A design diagram providing the required proof test levels as a function of desired lifetime and applied stress for the porous mullite is also presented.

17. Key Words (Suggested by Author(s))	18. Distribution Statement
Mullite, Porous, Ceramic Crack Growth, Fracture Toughness	Unclassified - Unlimited Subject Category 27

19. Security Classif. (of this report)	20. Security Classif. (of this page)	21. No. of pages	22. Price
Unclassified	Unclassified	24	

NASA FORM 1626 OCT 86